BIOLOGICAL
CRYSTALLOGRAPHY

Volume 71 (2015)

Supporting information for article:

Time-lapse anomalous X-ray diffraction shows how Fe^{2+} substrate ions move through ferritin protein nanocages to oxidoreductase sites

Cecilia Pozzi, Flavio Di Pisa, Daniela Lalli, Camilla Rosa, Elizabeth Theil, Paola Turano and Stefano Mangani

S1. Rationale for use of time-lapse anomalous diffraction for studying the iron pathways in ferritin

The cubic crystal form of RcMf, obtained by using $MgCl_2$ as precipitant (Tosha *et al.*, 2010), was chosen for this study because the superior diffraction quality of this crystal form allows atomic or near-atomic resolution structure determination. In addition, $[Mg(H_2O)_6]^{2+}$ ions slows down iron mineralization in RcMf, by blocking formation of the diferric peroxide catalytic intermediate (Liu & Theil, 2004), as shown by stopped-flow kinetic measurements obtained upon Fe^{2+} addition to protein solutions preincubated with Mg^{2+} in high concentration (see next paragraph). The combination of high resolution crystal structure determinations with freezing techniques provides the opportunity to study the evolution in time of iron binding at different ferritin sites within the crystals. To achieve this, we have exposed the crystals of RcMf and of the H54Q variant to crystalline ferrous ammonium sulfate powder (Mohr's salt) and allowed free diffusion of iron in the crystallization drop. Crystals frozen at different time intervals (1, 2, 5, 15, 30, 60 minutes) after exposure to iron were then examined.

X-ray crystallography provides a time and space average picture of molecules in the crystals. In the case of the RcMf cubic form used here, the average extends over the 24 subunits of the molecule represented by the single subunit present in the crystal asymmetric unit. The technique of free iron diffusion from the solid Mohr's salt to the ferritin crystal followed by flash freezing, allows trapping of intermediates along the iron pathways and allows observation of accumulated rate-limited species. The time lapse between the crystallographic determinations allows appreciating the succession of binding events that eventually lead to thermodynamic equilibrium. Furthermore, we have conducted our experiments at high pH (8.0) where we know, by previous kinetic measurements, that the turnover from ferrous to ferric oxide species is about two orders of magnitude higher than at neutral pH (Liu & Theil, 2004). This means that under these conditions, the rate limiting step of the overall ferritin catalyzed reaction is not the formation of the mineral ferric oxide, but instead is the binding of the ferrous ion substrate to the OS. Hence, our methodology is suited to follow the travel of ferrous ions inside RcMf by using anomalous diffraction.

When possible, we have performed two-wavelength anomalous diffraction experiments in order to ascertain the type of heavy atoms present in the crystal. We have collected data at the Fe K-edge peak energy and just below the Fe K-edge on the same crystal. The anomalous difference maps obtained, allow to safely distinguishing Fe from Mg, Cl or S atoms/ions (or any other atom lighter than iron, accidentally present in the crystal).

We have been also careful in choosing crystals of very similar size for all experiments, in order to avoid possible bias in comparisons coming from different iron diffusion kinetics inside the crystal (see Figure S3).

S2. High resolution structure of iron-free RcMf

The crystal structure of iron-free RcMf refined to 1.16 Å resolution (PDB code: 4LQH) was used as a reference structure. The resolution is higher than that of earlier RcMf structures and provides insights into the mobility present in the protein. The overall structure is very similar to others, such as PDB 3KA3

obtained at 1.4 Å resolution (Tosha *et al.*, 2010), the RMSD between the two structures, calculated on all Cα atoms being only 0.12 Å. Three magnesium ions from the crystallization solution are bound to the RcMf subunit OS at the same locations previously observed in the 3KA3 structure. Two of these metal ions (Mg1 and Mg2 in Figure 1 time zero main text) are bound with partial occupancy close to the iron binding sites seen in the iron-bound RcMf low resolution structures (Bertini *et al.*, 2012) (PDB codes: 3RBC, 3RGD), but at positions different from iron (see below and Figure 1, time 0 main text). The positions and the number of the Mg^{2+} ions observed here differ from those reported in the early structure of RcMf obtained at very low pH (4.5) in the trigonal form (PDB code: 1MFR) (Ha *et al.*, 1999). The partial occupancy of the magnesium ions is indicated by the refinement of thermal and occupancy factors, by the impossibly short apparent metal-metal distance (2.41 Å) (Yang *et al.*, 2008), and by the multiple conformations observed for the side chains of the metal binding residues His54, His61, Glu103 and Gln137. The observed static disorder is due, at least in part, to the different conformations of the residues occurring in the 24 subunits of RcMf that superimpose in the F432 crystal form of RcMf whose symmetry tolerates such small deviations.

A third Mg^{2+} ion (Mg3 in Figure 1, time 0 main text) is bound by Glu57, Asp140 and by Glu136 and bridged to one of the Mg^{2+} in the enzyme sites. Water molecules complete the Mg3 coordination sphere. Two other Mg^{2+} hexa-aqua ions are found in the 3-fold channel and H-bonded to Asp127, Ser131 and Glu130, coincident with two of the three Mg^{2+} ions found in the same channel of 3KA3. Finally, other three Mg^{2+} ions are found bound to the protein surface. The 4-fold channel defined by the four symmetry-related His169, does not contains metal ions but only chloride from the crystallization solution as indicated by the anomalous signal present there and by the non-coordinating position taken by the side chain of His169 (see Figure 5, main text).

S3. High resolution structure of Fe-RcMf: one minute free diffusion

The structure of RcMf crystal kept in contact with Mohr's salt powder for 1 minute has been refined to 1.27 Å resolution (PDB code: 4LPJ). The anomalous difference map calculated with phases from the refined model of iron-free RcMf shows a sharp peak at 7.6 σ located at the position of Fe1 in the RcMf OS while the Fe 2 site (see Figure 1, time 1, main text) appears empty with a Mg^{2+} ion bound in close proximity as in iron-free RcMf. The Fe1 occupancy has been refined to 0.30. Fe1 is coordinated to one of the two observed conformations of the side chains of Glu23 and His61 (30% bound, 70% unbound). The side chain of Glu58 appears ordered and bridges Fe1 to one water molecule which is part of the coordination sphere of one of the two Mg^{2+} ions that are still bound at partial occupancy in the same sites observed in iron-free RcMf. A third Mg^{2+} ion sits in the cavity, bound (partial occupancy) to the side chains of Glu103, Asp140 and water molecules. The His54 side chain is disordered over two positions. No other iron atoms are detected bound to RcMf. The 4-fold axis channel is occupied by chloride anions as in iron-free RcMf and 3KA3. The same two Mg^{2+} aqua-ions observed in iron free RcMf, are located into the 3-fold channel.

S4. High resolution structure of Fe-RcMf: two minutes free diffusion

The crystal structure of RcMf, after two minutes of free diffusion from Mohr's salt, has been refined to 1.20 Å resolution (PDB code:4LQJ). The anomalous difference Fourier map now shows two large peaks (13 σ for site 2 and 26 σ for site 1) indicating the presence of both iron atoms lodged in the proper sites in the OS, but with different, partial occupancy (Figure 1, time 2, main text. Table S1). The Fe1 occupancy refines to about 0.50 and that of Fe2 to 0.30. There is still trace of Mg^{2+} ions bound to their positions in the OS, as observed in the previous structures (not shown in Figure 1, time 2, main text). The Fe1-Fe2 distance is 3.63 Å and the Fe^{2+} ions are bridged by the side chain of Glu58, now observed in two conformations. One bridging the two iron ions and identical to that found in the structure of iron free RcMf, where it is hydrogen-bonded to the Mg^{2+} solvation sphere. A water species (one of the possible protonation states of water: $H_2O/OH^-/O^{2-}$ that cannot be specifically identified by the structural analysis, is indicated as Wat or Wb in all text and figures), most probably hydroxide, forms a second bridge between irons. Fe1 displays square pyramidal geometry, as in the 1 minute structure. The Fe2 ion is bound to Glu58 (bridging it to Fe1) and to Glu103 as symmetric bidentate ligand. Fe2 coordination is completed Wb and by a terminal water molecule. The geometry of the Fe2 site is irregular, somewhat between a square pyramid and a trigonal bipyramid, with angles and planes closer to those of the bipyramid (if the symmetric bidentate Glu103 carboxylate is considered as only one ligand).

The disorder present in the active site has not been detected in the previous structures and many side chains have multiple conformations difficult to model. Besides Glu58, also Glu23, His54, His61 and the more distant Met19 and Glu57 are disordered. The partial occupancy of the metal sites in the OS most probably indicates that Mg^{2+} ions are bound to a fraction of the molecules in the crystal while Fe^{2+} ions are bound to others. Indeed, whereas the distance of Fe site 1 from the closest Mg^{2+} ion (3.20 Å) is barely compatible with simultaneous presence of the two cations in the same OS, that of Fe^{2+} site2 (2.14 Å) is not.

Three anomalous peaks are aligned along the channel corresponding to the 4-fold axis. Of these, only one is missing in the anomalous map calculated from data collected at 7050 eV, below the iron edge, thus demonstrating that one iron ion is bound to the four His169 that define the entrance of the channel (see below and Figure 5, main text). The iron binding is also indicated by the two conformations observed for the side chains of His169: one is the same seen in the previous two structures, while the other brings the His169 Nε2 at coordination distance (2.43 Å) from iron. The other two anomalous signals present on the axis are still present in the low-energy anomalous map and have been interpreted as chloride anions that nicely superimpose to the chloride anions found in the iron free RcMf and 3KA3 structures. The coordination of iron on the 4-fold axis is not perfectly defined, as the partial occupancy of Fe and of the two chloride ions makes difficult to find the water molecule(s) completing the iron coordination sphere. One Mg^{2+} hexa-aqua ion sits in the 3-fold channel where it is H-bonded to Glu130. Further six Mg^{2+} ions complete the metal content of the ferritin molecule at positions corresponding with those of the Mg^{2+} ions found in 3KA3. We have also obtained a RcMf structure after five minutes of iron free diffusion (PDB code: 4LYX) that shows the same structural features of the two minutes structure.

S5. Structure of Fe-RcMf: 15 minutes free diffusion

The crystal structure of RcMf after fifteen minutes exposure to Fe^{2+} was refined to 1.90 Å resolution (PDB code: 4LYU). The OS of RcMf is occupied by two Fe^{2+} ions still at partial occupancy (about 0.70 for both Fe1 and Fe2). However, the coordination sphere of Fe1 is fully defined (see Figure 1, time 15, main text). Fe1 displays square pyramidal geometry with Glu23 (monodentate), the bridging Glu58, the bridging water (Wb in Figure 1, time 15, main text) and one terminal water molecule composing the basal plane, while His61 occupies the apex at a distance of 2.41 Å. The square-pyramidal geometry of the Fe 1 binding site of RcMf appears to be dictated by the presence of Val 106, conserved in catalytically active eukaryotic ferritins, at about 4.0 Å. Val106 position hinders the binding of a sixth ligand to Fe1.

The Fe2 ion is bound to Glu58 (bridging) and to Glu103 as symmetric bidentate ligand. The remaining electron density around Fe2 is more difficult to interpret. This is due to the presence of weaker, albeit significant, maxima in the anomalous difference map that are close to Fe2 (Figure 1 time 15, main text). One of them (4.0 σ), at about 2.5 Å from Fe2, can be interpreted as a Fe^{2+} ion (Fe3 in Figure 1, time 15) bound to the Nδ1 atom of His54 (site 3 in Figure 1 all sites). The short distance and the incomplete coordination sphere, indicate that Fe2 and Fe3 cannot be simultaneously bound to RcMf but rather indicate the iron approach to the OS. A second anomalous peak (5.0 σ; Fe4) is located between the side chains of Glu57 and Asp140, with the two carboxylate groups binding as bidentate ligands (site 4 in Figure 1 all sites). Wb (probably hydroxide) forms a second bridge to Fe1 and a terminal water molecule is clearly visible within coordination distance to Fe2. The Fe2 coordination sphere is not fully defined due to the anomalous peaks described above that occupy positions of potential ligands. More distant amino acids within the active site appear ordered, which may depend on the lower resolution of this structure determination (1.90 Å) compared to the near atomic resolution (1.2-1.3 Å) attained in the structure at 1 and 2 minutes. However, even after 15 minutes of exposure to iron, some disorder is present in the Fe2 coordinating waters, observed as diffuse maxima in the Fourier difference map.

The positions and the protein ligands of Fe1-Fe4 remarkably coincide with those of the four Co^{2+} ions found bound to the OS in the RcMf crystal structure (PDB code: 3KA4) recently reported by Tosha et al. Contrarily to the previous structures, there is no trace of Mg^{2+} ions bound into the OS.

One iron ion is consistently found on the 4-fold axis pores, coordinated into the plane of the four symmetry-related His169. Fe displays square-bipyramidal coordination geometry with one chloride anion at one of the apices and one water molecule at the other, facing the ferritin cavity (see Figure 5B, main text). The presence of the chloride anion is demonstrated by the signal present in this site in the anomalous difference map, obtained from data collected at energy below the Fe K-edge. The 3-fold axis channels are occupied by two Mg^{2+} aqua-ions. The anomalous difference Fourier map does not show any trace of iron ions, emphasizing the transient nature of iron-protein interactions at these locations. Only non-substrate metal ions such as Mg^{2+}, Zn^{2+}, Cu^{2+} and Co^{2+} may form stable metal protein bonds in ferritin ion 3-fold channels as observed in other in previously reported ferritin structures (Bertini *et al.* 2012; Tosha *et al.*, 2010; Toussaint *et al.*, 2007).

S6. Structure of Fe-RcMf: 30 and 60 minutes free diffusion

The crystal structure of RcMf obtained after 30 minutes of iron free diffusion has been refined to 1.54 Å resolution (PDB code: 4LQV). At this stage, the OS is well defined (Figure 1, time 30, main text), but the occupancy of the two iron sites is still partial (about 0.50 and 0.30 for site 1 and 2, respectively; Table S1). Moreover, the overall occupancy of the two sites decreased with longer exposure time suggesting that, during the exposure to iron, turnover occurs at both Fe1 and Fe2 sites.

Fe1 displays the same coordination observed in the 15 minutes structure while the anomalous peaks present in the surroundings of Fe2 in that structure are now absent. The Fe2 coordination is much better defined than in previous structures and can be described as a distorted trigonal bipyramid, where the Glu58 Oε2 and one terminal water occupy the apical positions while the symmetric bidentate Glu103 carboxylate (considered as one ligand), Wb and a further terminal water lie in the basal plane as shown in Figure 1 time 30 (main text).

The Fe2-Glu58 Oε2 distance results quite short (1.82 Å), but still well within the standard Fe^{2+} or Fe(III)-carboxylate distances (Harding, 1999; Orpen *et al.*, 1989). The Fe1-Glu58 Oδ1 and the Fe1-Fe2 distances are 1.97 Å 3.62 Å, respectively.

The 4-fold channel hosts the same iron ion observed in the previous structures exactly in the same coordination environment. Mg^{2+} aqua-ions are bound to the 3-fold channel at the same positions observed in previous structures.

The crystal structure obtained after 60 minutes of treatment with the iron salt (PDB code: 4LQN) shows that metal-ferritin interactions remain unchanged with respect to 30 minutes, indicating that equilibrium binding was achieved in the crystals between 15 and 30 minutes lapse. Sites Fe1 and Fe2 remain only partially occupied at a lower value (about 0.50). The Fe-Fe distance is now 3.54 Å.

The 60 minutes exposure to iron was repeated for a crystal obtained with the same precipitant ($MgCl_2$), in the same cubic crystal form, but at pH 6.5 instead of pH 8.0. This has been done to check the influence of pH on the iron uptake by RcMf, and to have a comparison with the trigonal, low resolution structure obtained from crystal grown in formate at neutral pH (Bertini *et al.*, 2012). This structure of RcMf has been determined at 2.04 Å resolution. The OS shows two iron atoms bound at about 0.40 occupancy. However, they are now only 3.15(5) Å apart, bound to the same residues observed in the other structures and bridged by a water species, confirming the observation already obtained from the low resolution structure of the trigonal form of RcMf (Bertini *et al.*, 2012). The short Fe-Fe distance is characteristic of diferric μ-oxo/hydroxo clusters (Orpen *et al.*, 1989).

S7. The effects of removing environmental dioxygen on the structure of Fe-RcMf.

The structure of RcMf (PDB code 4MY7) has been obtained at 1.48 Å resolution from crystals treated with Fe^{2+} (as Mohr's salt) in the absence of the second substrate dioxygen and exposed to the ferrous salt for about three minutes (see the Methods section). The anomalous difference Fourier maps obtained from data at and below the Fe K-edge (7130 eV) clearly show the presence of four iron ions in the OS (see Figure 2).

Both the Fe1 and Fe2 sites are partially occupied by iron ions (estimated occupancies of about 0.90 and 0.50, respectively); the Fe-Fe distance is 3.64 Å, comparable with those observed in air exposed crystals (Table S2). The coordination geometry of Fe1 is the same regular, square-pyramid reported for the previous structures. However, the Fe2 site shows the carboxylate group of Glu103 bound to iron in two conformations: bidentate symmetric and bidentate asymmetric (see Figure 2, main text). The coordination sphere of Fe2 contains also Glu58, the bridging water species to Fe1 (Wb) and a second water species (Wb2), but complete definition of the Fe2 coordination is hampered by a large, anomalous peak due to an iron at 3.32 Å from Fe2. This is a third iron ion, Fe3 (site 3 Figure 1 all sites, main text), that refines to about 0.40 occupancy and appears bound to one conformation of Glu103 (as monodentate, bridging it to Fe2), to His54, Glu57, Asp140 and to Wb2 that forms a second bridge to Fe2 (Figure 2, main text). A terminal water molecule completes the ligands of Fe3. The side chain of His54 appears disordered with a second conformation that brings it at bonding distance to Fe2, but the modeling is hindered by the presence of the electron density due to Fe3. It should be noted that the anomalous difference map obtained at the Fe K-edge shows a continuous stretch of anomalous density elongating from Fe3 and reaching the Fe2 maximum. This observation, together with the disorder and the partial occupancy of the iron sites indicates a pathway for Fe to ferritin OS assisted by the conformational variability of His54, in agreement with the observation made on the cobalt and copper adducts of RcMf (Bertini *et al.*, 2012; Tosha *et al.*, 2010). A fourth iron ion, Fe4 (site 4 Figure 1 all sites, main text), is located at 3.63 Å from Fe3 and refines to 0.20 occupancy. It appears bound to Glu57, Glu136, Asp140 (bidentate) and two terminal waters. It is interesting to note that the Fe3 and Fe4 coordination polyhedra are respectively, a quite regular octahedron and trigonal bipyramid (Figure 2, main text). Fe4 is located on the inner surface of the ferritin cavity.

The possible presence of some of the Fe binding sites near/at ferritin OS was already suggested by the earlier studies of ferritin-Co^{2+} and ferritin Cu^{2+} co-crystals (Bertini *et al.*, 2012; Tosha *et al.*, 2010).

S8. Effect of amino acid substitution near the OS of ferritin

The protein environment near enzyme sites can play an important role in directing substrate to the OS. In the case of ferritin, metal ions have been observed bound near the active sites, such as to His 54 in the RcMf structures presented here and in our previous work (Bertini *et al.*, 2012). Gln58 in human H chain takes the structural position of RcMf His54. In order to investigate the effect of the substitution on the iron binding, theRcMf-H54Q variant was created, isolated and crystallized under the same conditions as wt-RcMf. The iron-free RcMf-H54Q crystal structure has been determined at 1.30 Å resolution (PDB code: 4MKU). Comparison with wt-RcMf and HuHf crystallized in the same conditions (PDB codes: 4LQH and 3AJO (Masuda *et al.*, 2010)) show very small deviations among the three structures (RMSD less than 0.35 Å, calculated on the common Cα atoms). Sequence identity between HuHf and RcMf or RcMf-H54Q is only 64 % confirming the similarity of ferritin protein crystal structures for sequence variations of up to 80% (Crichton & Declercq, 2010). However, RcMf-H54Q shows significant changes in the OS if compared to wt-RcMf. In contrast to wt-RcMf, one Mg^{2+} ions is bound to the Fe1 site in an unexpected square-pyramidal

coordination lacking the sixth ligand (Figure 3 time 0, main text). Five coordinate geometry is seldom observed for Mg^{2+}. However, some examples of square-pyramidal carboxylate bound Mg^{2+} ions are present in the PDB (Harding & Hsin, 2014). The Fe1 site is empty in the wt-RcMf iron free structure, but occupied by a Mg^{2+} ion in human ferritin (3AJO). The second Mg^{2+} ion of RcMf-H54Q is bound to the side chain of Gln54 and corresponds to the Mg^{2+} ion bound to Gln58 in 3AJO. Again, this site is empty in wt-RcMf. These findings indicate that the H54Q mutation renders the OS of RcMf very similar to that of HuHf.

S9. Structure of RcMf-H54Q variant: 1 min free diffusion

The OS of RcMf-H54Q treated for 1 minute with Mohr's salt, shows a quite complex picture (Figure 3, time 1, main text; PDB code: 4ML5). The anomalous difference map (computed with data collected just above the Fe K-edge at 7130 eV) clearly shows one Fe^{2+} ion bound to site 1 at high occupancy (0.70) in square pyramidal geometry (His61 apical, Glu23 and Glu58 and 2 water molecules in basal plane) while the Fe2 site is empty. One Fe^{2+} ion is bound with partial occupancy to the Fe3 site. This metal binding site is the Fe3 site already observed in the 15 minutes wt-RcMf structure and in the O_2-free wt-RcMf structure (see Figure 1, time 15 and Figure 2, main text). The anomalous difference map, computed with data collected above the iron edge, shows the presence of two further iron peaks (that disappear in the anomalous map computed with the data collected below the iron edge at 7080 eV). Such peaks can be attributed to Fe^{2+} ions bound at partial occupancy to sites that lie just outside of the OS. One of these irons is bound to the side chains of Glu57 and Asp140, in one of the two different conformations observed in this structure, and to water molecules. This iron site is the Fe4 also observed in the 15 minutes and O_2-free RcMf structures (see Figures 1 time 15 and 2, main text). One of the waters bridges it to the Mg^{2+} bound to the described Gln54 site. The second Fe^{2+} ion occupies a new iron binding site (Fe5 site in Figure 3 time 1, main text) where it is bound to one of the conformers of the Glu53 and Glu57 side chains in a quite regular octahedral geometry completed by water molecules, one of which bridges it to the previous Fe4 ion. Both the Fe4 and Fe5 sites are located in the inner surface of the ferritin, facing the cage cavity.

S10. Structure of Fe-RcMf-H54Q variant:15 min free diffusion

The structure of RcMf-H54Q variant treated for 15 minutes with Mohr's salt shows an unprecedented view of the OS (Figure 3, time 15, main text; PDB code: 4MN9). Four large peaks (above 14.0 σ) of different height appear in the anomalous difference map obtained from data just above the iron edge (7130 eV) which are absent from the map collected below the edge. The largest peak (71.2 σ, 0.80 occupancy) corresponds to the Fe1 site where Fe is bound in the already described square pyramidal coordination geometry. The Fe2 site shows a weaker peak (15.0 σ) corresponding to a Fe^{2+} ion that refines to 0.30 occupancy.

The coordination geometry of the Fe2 ion is now slightly different from that observed for the Fe2 ion in the structure of wt-RcMf treated for the same time. The Fe2 geometry can be described as a distorted square pyramid with the basal plane consisting of the Glu58 Oε2, Wb that bridges it to Fe1 and two further water

molecules; the apex is occupied by the symmetric bidentate Glu103 carboxylate group (considered as a single ligand; Figure 3, time 15, main text). The Fe1-Fe2 distance is now 3.80 Å.

Two further large anomalous peaks (17.4 σ and 18.2 σ, respectively) and one weaker peak (5.2 σ) indicate the presence of other iron ions in the cavity. Most of the protein ligands involved in these sites show double conformations, namely Glu53, Gln54, Glu57 and Asp140. The third Fe site (Fe3) is distorted octahedral with the basal plane constituted by two water molecules, Glu103 Oε2 and Asp140 Oδ2 (in one of the two conformations). The apices are Gln54 Oε1 (one of the two conformations) and a water molecule. Fe3 is triply bridged to Fe2 by the two Wb and by Glu103 Oε2, at the very short distance of 2.84 Å from Fe2. The fourth Fe^{2+} ion (Fe4) is bound to a nearby site constituted by Gln54 (one of the two conformations), a bidentate Asp140 (one of the two conformations) and Glu136 Oε2 as protein ligands, the Wb bridge to Fe3 and two terminal waters. The Fe3-Fe4 distance is 3.67 Å.

In summary, the OS cavity is occupied, on average, by a cluster of four iron ions bridged by a series of protein and water/hydroxide ligands as shown in Figure 3 time 15 (main text). There is trace of a fifth Fe^{2+} ion (Fe5) given by a weak anomalous peak just above noise (5.0 σ) that sits in a site close to Fe3 and bound to the side chain of Gln54 (one conformation), Glu57 (one conformation) and by water molecules. This is the same site observed in RcMf-H54Q at one minute. The Fe4 and Fe5 sites lie just inside the ferritin cage. Fe5 has no counterpart in wt-RcMf.

The scenery depicted in this structure is complicated by the partial occupancy of the sites. Indeed, while Fe1 occupancy refine to about 0.80, those of Fe2, Fe3, Fe4 and Fe5 range from 0.40 to 0.25 as do the water molecules bound to them. Furthermore, the side chains of three protein ligands of the cluster (Gln54, Glu57, Asp140) are observed in double conformations. As a consequence, the Fe2-Fe3-Fe4 cluster and Fe5 ion most probably do not represent a structure that occupies these sites in all RcMf-H54Q subunits, but rather indicate a superposition of different states that are due to a dynamic process of the iron interaction with the protein. This is indicated by the multiple conformations adopted by Glu53, Glu57 and Asp140 that are bound to different iron ions and appear to handle the metal ions from one site to the next one in a sort of a movie. The Fe sites in this structure are completed by a sixth Fe^{2+} ion bound, as always, into the 4-fold channel in square-bipyramidal geometry by the four His 169 Nε2, a chloride anion and a water molecule. Mg^{2+} ions occupy the 3-fold axis channel.

S11. Structure of Fe-RcMf-H54Q variant: 60 min free diffusion

The structure of RcMf-H54Q treated for 60 minutes with Mohr's salt shows the OS occupied by four Fe^{2+} ions (Figure 3, time 60, main text; PDB code: 4MJY). Fe1 and Fe2 are indicated by large peaks (18.2 and 16.0 σ, respectively) in the anomalous difference map calculated from data collected at the iron absorption peak (7130 eV) which are absent from the map collected below the edge (7040 eV). The occupancies of these irons refine to about 0.60 and 0.40 for Fe1 and Fe2, respectively. A third Fe site (Fe3, 10.6 σ) is now located in between the positions of the Fe3 and Fe4 in the RcMf-H54Q 15 minutes structure. Fe3 is bound to one of the conformers of Glu57 and Glu136 and to Asp140 (one conformation) and is at 3.1 Å from Gln54

(one conformation). A water molecule bridges Fe3 and Fe2 located at 3.85 Å. A fourth, very weak peak (7.0 σ) indicates the presence of a Fe4 ion bound to two conformers of Glu57 and Glu136 at 3.35 Å from Fe3. The Fe3 and Fe4 positions are slightly different from those observed for the corresponding ions in the 15 minutes structure, suggesting a movement of the Fe3 and Fe4 ions assisted by the amino acid side chains, in particular by that of Glu57.

An interesting feature of this structure is that an anomalous peak indicating the presence of iron is present in correspondence to the position of the Mg^{2+} hexa-aqua ion found in the 3-fold pores. This Fe^{2+} ion shows the regular octahedral structure of a Fe^{2+} hexa-aqua ion (Figure 4, main text). The Fe^{2+}-aqua ion is held by nine symmetric H-bonds to Asp127 and Glu130. This finding is the first structural evidence of the transit of Fe^{2+} aqua-ions through the ferritin 3-fold pores. Iron is present in the 4-fold pores in the same coordination environment already described.

The occupancy of the Fe1 site by iron is always greater (or equal) than Fe2 (Table S1) at all times, but never reaches 1.0 in the aerobic protein crystals. In this respect, it should be emphasized that our BfMf structures represent the average over 24 subunits of all molecules in the crystal. Hence, the different diffusion kinetics of the iron ions in the crystal could explain the observed fractional site occupancies. However, the occupancy of Fe1 reaches a maximum after 15 minutes in both wt-RcMf and in the H54Q variant and decreases after longer times of exposure to iron and dioxygen substrates, thus indicating turnover of the iron substrate in the crystals. Indeed, despite a large number of attempts made by us by loading RcMf with the stoichiometry of two, four or eight Fe^{2+} ions per subunit, we have never been able to observe occupancy of the Fe1 and/or the Fe2 sites. Only by supplying a continuous flux of iron and by freezing the crystals, we have been able to observe the binding of iron to wt-RcMf and its variant H54Q.

The observation of almost full occupancy of the Fe1 site in the anaerobically grown RcMf crystals (where turnover cannot occur; see Table S1) and of their cracking of after short exposure time to Fe^{2+} ions (three minutes), confirms the existence of turnover in the aerobically treated crystals.

S12. Stopped-flow measurements results

To study the effect of the substitution of RcMf His54 with Gln on iron oxidation rates, we compared the kinetics of the formation of diferric peroxo/oxo species in wt-RcMf and variants. The diferric peroxo complexes have a maximum absorbance at 650 nm, while many $Fe^{3+}O$ species (including diferric peroxo at the active sites, diferric-oxo product and Fe^{3+} multimers) absorb at 350 nm (Hwang *et al.*, 2000).The rates of formation of the diferric peroxo (A_{650nm}) and of the $[Fe^{3+}O]_n$ species(A_{350nm}) were derived from the change in absorbance as a function of time measured with rapid mixing, UV-vis spectroscopy (described in Methods, main text). The comparison of the progress curves acquired on the wild type ferritin and its variants shows that the catalytic activity of the protein is not affected by the substitution of Gln at position 54.

Similarly, to monitor the effect of the presence of Mg^{2+} on iron oxidation rate, the initial catalytic rates of demetallated and Mg^{2+}-loaded ferritin were measured. The calculated oxidation rate of $Fe^{2+}$is significantly decreased in presence of Mg^{2+}. Indeed, the rate of diferric peroxo formation (A_{650nm}) in Mg loaded ferritin is

850 times lower than that observed in absence of Mg^{2+} when 2 equivalents of Fe^{2+} were added (see Figure S1). Also the rate of the $[Fe^{3+}O]_n$ species formation (A_{350nm}) is 450 times lower in presence of Mg^{2+} (see Figure S2). Such behavior resembles the one observed for the RcMf variant E130A, where rates of diferric peroxo and (Fe^{3+} formation and are 600 and 100 times lower than those observed for the wild type protein (Haldar *et al.*, 2011).

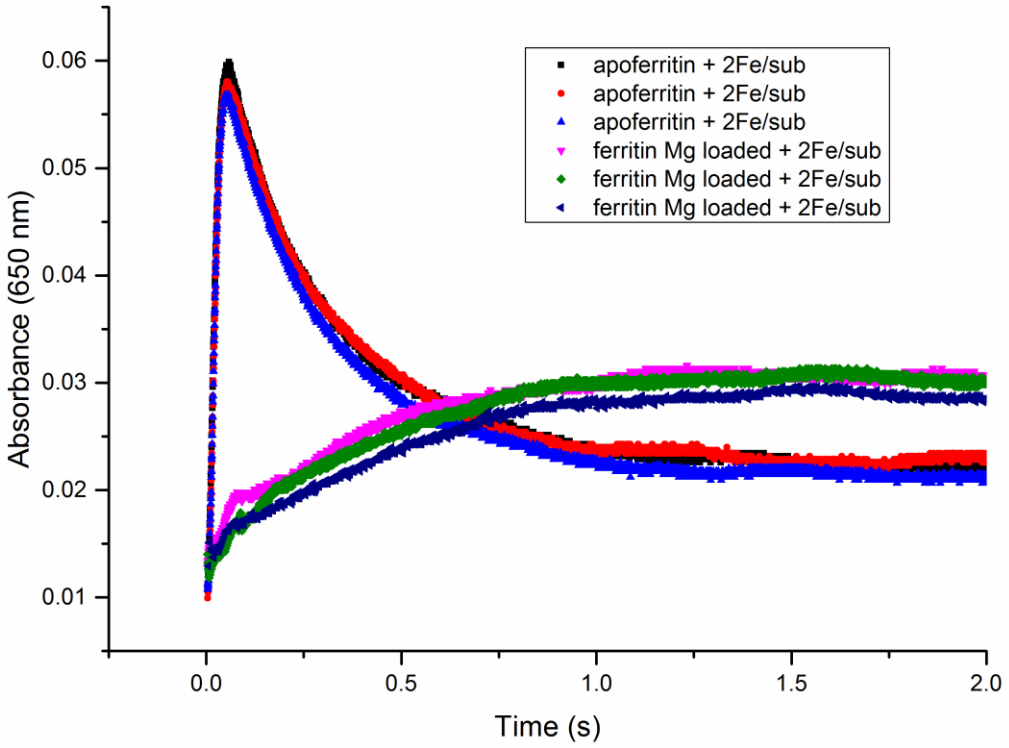

Figure S1 Kinetics of Fe^{2+} oxidation by wt-RcMf monitored by the change in absorbance at 650 nm. Each experiment has been repeated three times to check for reproducibility. The black, red and light blue absorbance curves were acquired after mixing demetallated ferritin with 2 Fe^{2+}/subunit, while those in blue, magenta and green were recorded after addition of 2Fe^{2+}/subunit to a solution of wt-RcMf containing 0.1M $MgCl_2$.

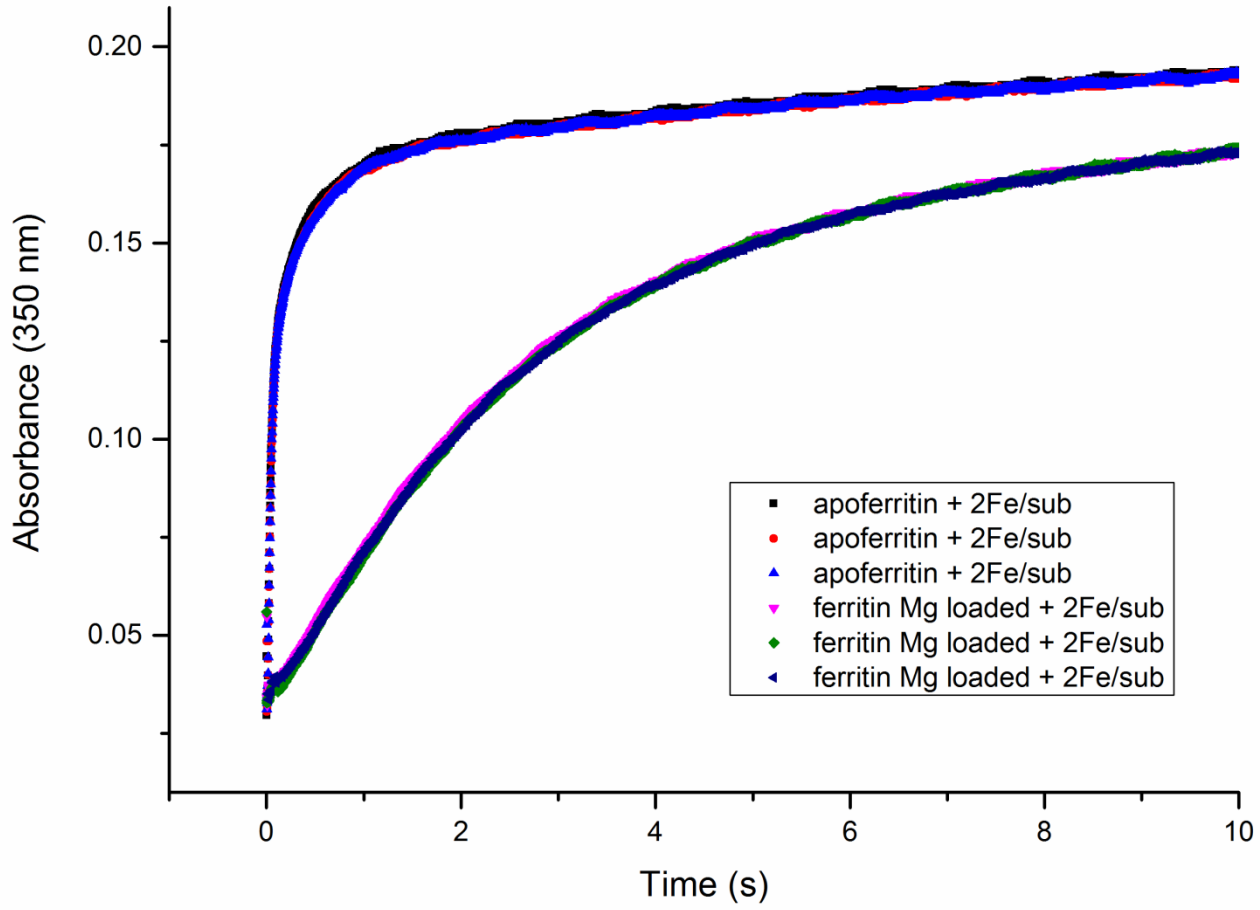

Figure S2 Kinetics of Fe^{2+} oxidation by wt-RcMf monitored by the change in absorbance at 350 nm. Each experiment has been repeated three times to check for reproducibility. The black, red and light blue absorbance curves were acquired after mixing demetallated ferritin with 2 Fe^{2+}/subunit, while those in blue, magenta and green were recorded after addition of 2Fe^{2+}/subunit to a solution of wt-RcMf containing 0.1M $MgCl_2$.

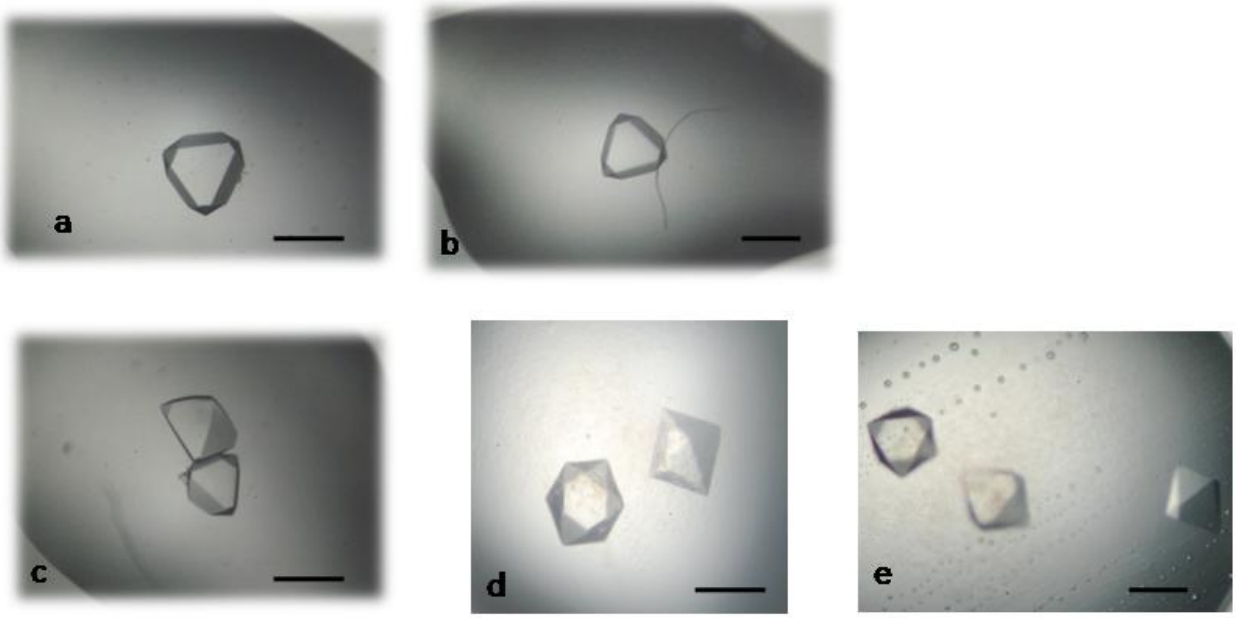

Figure S3 Crystallization drops of wt-RcMf and RcMf-H54Q (d) showing the reproducible, similar size of the cubic crystal form obtained under our conditions. Bars indicate 0.15 mm.

Table S1 Variation in time of iron fractional occupancies in sites 1 and 2 (rows 2-3) and of the Fe-Fe distances (Å; row 4) in the RcMfOS.

The PDB codes of each structure are reported. The ESDs of Fe1-Fe2 distances are given in parentheses.

Fe sites	RcMf 1min 4LPJ	RcMf 2 min 4LQJ	RcMf 5 min 4LYX	RcMf 15 min 4LYU	RcMf 30 min 4LQV	RcMf 60 min 4LQN	RcMf O_2 free 3 min 4MY7	RcMf-H54Q 1 min 4ML5	RcMf-H54Q 15 min 4MN9	RcMf-H54Q 60 min 4MJY
Fe1	0.30	0.50	0.50	0.70	0.50	0.50	0.90	0.70	0.80	0.60
Fe2	-	0.30	0.30	0.70	0.30	0.50	0.50	-	0.30	0.40
Fe1-Fe2	-	3.63(2)	3.64(3)	3.76(7)	3.62(5)	3.54(6)	3.64(5)	-	3.80(2)	3.58(4)

Table S2 Fe-Fe distances in di-iron model compounds crystal structures.

References in parentheses.

Di-iron sites models	Fe-Fe distance (Å)
Fe(III)-Fe(III) μ-oxo-μ-dicarboxylate	3.15-3.17 (Armstrong *et al.*, 1984; Feng *et al.*, 1989)
Fe(II)-Fe(II)μ-formate-μ-dicarboxylate	3.58 (Tolman *et al.*, 1989)
Fe(III)-Fe(III)μ-hydroxo-μ-dicarboxylate	3.44 (Armstrong & Lippard, 1984)
Fe(III)-Fe(III)μ-dihydroxo	3.08-3.09 (Thich *et al.*, 1976)
Fe(III)-Fe(III)μ oxo-μ carboxylate	3.20-3.24-3.26 (Norman *et al.*, 1990b; Norman *et al.*, 1990a)

Table S3 The effect of altering the properties of the 3-fold channel on different ferritins.

Ferritin type	3-fold channel variant	Effect	Rationale	References
BfMf	E130A	Abolishes DFP formation; reduces formation rate of ferric oxo species.	Hindered Fe(II) guidance to OS	(Haldar *et al.*, 2011)
	E130I	Reduces DFP formation; reduces formation rate of ferric oxo species.	Hindered Fe(II) guidance to OS	(Behera & Theil, 2014; Haldar *et al.*, 2011; Theil *et al.*, 2014)
	D127A	Abolishes DFP formation at low Fe(III) load; reduces formation rate of ferric oxospecies. Lesser effect of DFP formation at higher Fe(II) load	Hindered Fe(II) guidance to OS	(Behera & Theil, 2014; Haldar *et al.*, 2011; Theil *et al.*, 2014)
	R72D	DFP formation similar to WT; reduces DFP stability; slighthly faster formation rate	Altered distribution of negatively charged residues along the 3-fold channel	(Tosha *et al.*, 2012a; Tosha *et al.*, 2012b)

		of ferric oxo species. Increases caged-iron exit.		
	D122R	Reduces DFP formation; reduces DPF stability; reduces formation rate of ferric oxo species. Increases caged iron exit.	Changes in 3-fold channel structure/disorder.	
	L134P			
HuHf	E134A	Reduces formation rate of ferric oxo species and amount of iron incorporation.	Reduced diffusion through 3-fold channel.	(Levi *et al.*, 1996)
	D131A+E134A	Reduces formation rate of ferric oxo species and amount of iron incorporation.	Reduced diffusion through 3-fold channel.	(Levi, *et al.*, 1996)
	D131I + E134F	Reduces formation rate of ferric oxo species and amount of iron incorporation; eliminates Tb(III) binding;absence of fluorescence quenching on a Trp engineered near the ferroxidase center.	Reduced diffusion through 3-fold channel.	(Bou-Abdallah *et al.*, 2003)
	H118A	Small reduction of formation rate of ferric oxo species at OS iron incorporation; no effect on Tb(III)		(Bou-Abdallah *et al.*, 2003)

		binding.		
	H128A	No effect on formation rate of ferric oxo species at OS; reduced iron incorporation; no effect on Tb(III) binding.		
	C90E+C102A+C130A	Small reduction of formation rate of ferric oxo species at OS and iron incorporation; no effect on Tb(III) binding.		
	D131H+E134H	penetration into the cavity of the negatively charged 4-carboxy-TEMPO radical which is excluded completely in WT HuHf	abolished negative charge allows penetration of anions	(Yang *et al.*, 2000)
Human L-chain ferritin (HuLf)	D131A+E134A	Reduced iron incorporation and Tb(III) binding.		(Levi *et al.*, 1996)
Soybean seed H2f *	E165I+E167A+E171A	Partial reduction of formation rate of ferric oxo species at OS.	Reduced diffusion through 3-fold channel, while diffusion through the 4-fold channels is still active	(Lv C *et al.*, 2014)

* In plant ferritins both the 3-fold and 4-fold channels are active in iron import.

References

Armstrong, W. H., Spool, A., Papaefthymiou, G. C., Frankel, R. B. & Lippard, S. J. (1984). *J. Am. Chem. Soc.* **106**, 3653-3667.

Armstrong, W. H. & Lippard, S. J. (1984). *J. Am. Chem. Soc.* **106**, 4632-4633.

Behera, R. K. & Theil, E. C. (2014). *Proc. Natl. Acad. Sci. U. S. A.* **111**, 7925-7930.

Bertini, I., Lalli, D., Mangani, S., Pozzi, C., Rosa, C., Theil, E. C., & Turano, P. (2012). *J. Am. Chem. Soc.* **134**, 6169-6176.

Bou-Abdallah, F., Arosio, P., Levi, S., Janus-Chandler, C., & Chasteen, N. D. (2003).. *J Biol Inorg. Chem.* **8**, 489-497.

Crichton, R. R. & Declercq, J. P. (2010). *Biochimica et Biophysica Acta (BBA) - General Subjects* **1800**, 706-718.

Feng, X., Bott, S. G., & Lippard, S. J. (1989). *J. Am. Chem. Soc.* **111**, 8046-8047.

Ha, Y., Shi, D., Small, G. W., Theil, E. C., & Allewell, N. M. (1999). *J. Biol. Inorg. Chem.* **4**, 243-256.

Haldar, S., Bevers, L. E., Tosha, T., & Theil, E. C. (2011). *J Biol Chem.* **286**, 25620-25627.

Harding, M. M. (1999). *Acta Cryst. D* **55**, 1432-1443.

Harding, M. M. & Hsin, K. Y. (2014). *Methods Mol. Biol.* **1091**, 333-342.

Hwang, J., Krebs, C., Huynh, B. H., Edmondson, D. E., Theil, E. C., & Penner-Hahn, J. E. (2000). *Science***287**, 122-125.

Levi, S., Santambrogio, P., Corsi, B., Cozzi, A., & Arosio, P. (1996). *Biochem. J.* **317**, 467-473.

Liu, X. & Theil, E. C. (2004). *Proc. Natl. Acad. Sci. U. S. A.* **101**, 8557-8562.

Lv, C., Zhang, S., Zang, J., Zhao, G., & Xu, C. (2014). *Biochemistry* **53**, 2232-2241.

Masuda, T., Goto, F., Yoshihara, T., & Mikami, B. (2010). *Biochem. Biophys. Res. Commun.* **400**, 94-99.

Norman, R. E., Holz, R. C., Menage, S., Que, L., Zhang, J. H., & O'Connor, C. J. (1990a). Effects of the Fe-O-Fe angle. *Inorganic Chemistry* **29**, 4629-4637.

Norman, R. E., Yan, S., Que, L., Backes, G., Ling, J., Sanders-Loehr, J., Zhang, J. H., & O'Connor, C. J. (1990b). *J. Am. Chem. Soc.* **112**, 1554-1562.

Orpen, G., Brammer, L., Allen, F. H., Kennard, O., & Watson, D. G. (1989). *J. Chem. Soc. ,Dalton Trans.* S1-S83.

Theil, E. C., Turano, P., Ghini, V., Allegrozzi, M., & Bernacchioni, C. (2014). *J Biol. Inorg. Chem.* **19**, 615-622.

Thich, J. A., Ou, C. C., Powers, D., Vasiliou, B., Mastropaolo, D., Potenza, J. A., & Schugar, H. J. (1976). *J. Am. Chem. Soc.* **98**, 1425-1433.

Tolman, W. B., Bino, A., & Lippard, S. J. (1989). *J. Am. Chem. Soc.* **111**, 8522-8523.

Tosha, T., Ng, H. L., Bhattasali, O., Alber, T., & Theil, E. C. (2010). *J Am. Chem Soc.* **132**, 14562-14569.

Tosha, T., Behera, R. K., Ng, H. L., Bhattasali, O., Alber, T., & Theil, E. C. (2012a). *J Biol. Chem.* **287**, 13016-13025.

Tosha, T., Behera, R. K., & Theil, E. C. (2012b). *Inorganic Chemistry* **51**, 11406-11411.

Toussaint, L., Bertrand, L., Hue, L., Crichton, R. R., & Declercq, J. P. (2007). *J Mol. Biol.* **365**, 440-452.

Yang, T. Y., Dudev, T., & Lim, C. (2008). *J. Am. Chem. Soc.* **130**, 3844-3852.
Yang, X., Arosio, P., & Chasteen, N. D. (2000). *Biophys. J.* **78**, 2049-2059.